ChemComm

# Self-assembly of Chimeric Peptides Toward Molecularly Defined Hexamers with Controlled Multivalent Ligand Presentation



| | |
|---|---|
| Journal: | *ChemComm* |
| Manuscript ID | CC-COM-03-2020-002066.R1 |
| Article Type: | Communication |
| | |

COMMUNICATION

# Self-assembly of Chimeric Peptides Toward Molecularly Defined Hexamers with Controlled Multivalent Ligand Presentation†

Received 00th January 20xx,
Accepted 00th January 20xx

DOI: 10.1039/x0xx00000x

Xiushuang Yuan[a,b] , Linhai Jiang[c] , Weike Chen[b], Bo Song[d], Wei Chen[e], Xiaobing Zuo[f], Xiankai Sun[g], Xiaopeng Li[d], Kent Kirshenbaum[c], Shizhong Luo[a]*, He Dong[b]*

**This work demonstrates a self-assembling peptide strategy to form finite, molecularly defined trigonal bipyramidal-like hexamers which offer control over multivalent ligand display for enhanced tumor targeting.**

Generating discrete, soft nanostructures with precise control of size, geometry, and presentation of ligands toward cell-surface receptors offers tremendous opportunities for disease diagnosis and treatment.[1] The approach of supramolecular assembly has been effective to generate discrete assemblies by using orthogonal recognition strategies to program self-assembly.[2] Such principles have been well illustrated for the generation of intricate protein and DNA assemblies with defined molecular composition, 3D structures and functional features.[3]

As structural constituents of proteins, peptides can be *de novo* designed to fold into well-defined molecular structures, which can interact with one another to form highly ordered nanostructures and nanostructured networks.[4] In the past two decades, research has been primarily focused on the design of β-sheet forming peptides which can self-assemble into nanofibers of different length dimension. Recently, there have been remarkable advances in the design and fabrication of finite peptide assemblies with improved structural homogeneity. Among many notable examples, the Woolfson group developed a novel self-assembled coiled coil nanocage using two orthogonal coiled coil folding motifs.[5] The Jerala group demonstrated a single chain coiled coil polypeptide tetrahedron.[6] The Ryadnov group designed helical antimicrobial peptides which can self-assemble into a highly defined peptide capsid.[7] The Nowick group reported well-defined amyloid-like oligomers based on macrocyclic beta sheet peptides.[8] Using collagen mimetic peptides, the Conticello group constructed discrete 2-D sheets with exquisite control over both the short and long-range ordering.[9]

Inspired by the above studies and other advances in peptide design, particularly collagen mimetic peptide design and supramolecular assembly,[10] our group reported a new methodology to generate a finite peptide assembly using two distinctly folded protein motifs, *i.e.* a collagen triple helix and a coiled-coil dimer.[11] Previously, we showed side-to-side conjugation through a disulfide bond between the cysteine residue in the middle of each peptide led to well-defined hexamers or dodecamers while an end-to-side conjugate led to heterogeneous assemblies. For example, the collagen peptide $(POG)_2(PCG)(POG)_6$ (P: Proline; O: Hydroxyproline; G: Glycine; C: Cysteine), termed as P26 was used for side-to-side conjugation and its constitutional isomer, $(PCG)(POG)_8$, termed as P8 was used for end-to-site conjugation. Besides different conjugation geometry, the two peptides differed in the number of (POG) repeating units preceding the (PCG) conjugation site, which could be another important factor to drive the formation of finite structures. In a longer collagen peptide, such as P8, the larger number of POG units can increase the packing stability of the collagen trimers, however, suffer from packing specificity. They are likely to form kinetically trapped assemblies in particular when conjugated with another self-assembling coiled coil peptide. On the other hand, a shorter collagen peptide may not be as stable, but can enhance the packing specificity to form the most thermodynamically stable blunt-ended trimer, which is desired toward the formation of finite assemblies. In order to test this hypothesis, two shorter collagen peptides, named P7 and P6 were used to form end-to-side conjugates with a coiled-coil dimer peptide, termed as 26r. The chimeric conjugates were named as P7-26r and P6-26r (**Scheme 1**). In the current study, we focus on self-assembled hexamers because they have comparable molecular weights to single-chain variable fragments (ScFv) antibodies, which often show rapid tumor

[a.] *College of Life Science and Technology, Beijing University of Chemical Technology, Beijing,100029, China. E-mail: luosz@mail.buct.edu.cn*
[b.] *Department of Chemistry and Biochemistry, The University of Texas at Arlington, Arlington, TX 76019, USA. E-mail: he.dong@uta.edu*
[c.] *Department of Chemistry, New York University, New York, NY 10003, USA. E-mail:*
[d.] *Department of Chemistry, The University of South Florida, Tampa, FL 33620, USA*
[e.] *Department of Physics, The University of Texas at Arlington, Arlington, TX 76019, USA.*
[f.] *X-ray Science Division, Argonne National Laboratory, Lemont, IL 60439, USA.*
[g.] *Department of Radiology, The University of Texas Southwestern Medical Center, Dallas, TX 75390, USA.*
These authors made equal contribution to the work.
†Electronic Supplementary Information (ESI) available: Full experimental procedures and additional characterizations. See DOI: 10.1039/x0xx00000x

penetration.[12] Various peptide-based ligands for cell surface receptors can be readily incorporated on P7. As a proof-of-concept, we synthesized a chimeric peptide consisting of a RGDS ligand which can self-assemble into hexamers. *In vitro* tumor targeting efficacy of the hexamer was studied and compared with those of dimers or trimers which have only local ligand presentation, and hexamers without targeting ligands or with scrambled DGSR.

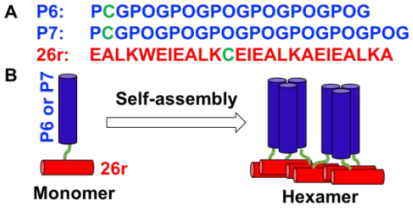


**Scheme 1.** (**A**) Sequences of the two domains in chimeric peptides, P6-26r and P7-26r. Single letter amino acid code representation. (**B**) Schematics of the self-assembly of an end-to-site conjugate to form a thermodynamically stable assembly in which the oligomerization state is defined by the Least Common Multiple (LCM) of the oligomerization states of two domains: 3 x 2 = 6.

Electrospray ionization-mass spectrometry confirmed the formation of hexamers with a series of peaks with continuous charge distributions (**Fig. 1A**). For instance, the peaks at m/z = 2270 and 2415 can be exclusively assigned to the hexameric assemblies of P6-26r and P7-26r with a charge of +13, respectively. Note that trimers were also observed likely due to fragmentation during mass spectrometry. The sigmoidal thermal transition curves confirmed the formation of collagen triple helix tertiary structures for free P6 and P7 in solution with a melting temperature at 35 °C for P6 and 48 °C for P7 (**Top traces** on **Fig. 1B** and **1C**). 26r also exhibited a sigmoidal thermal transition profile suggesting the formation of coiled coil tertiary structures (**Fig. S2**).

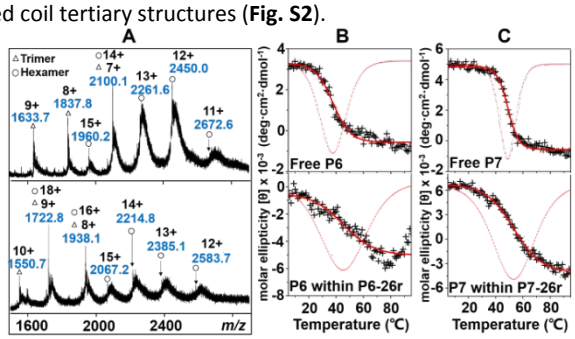


**Figure 1.** (**A**) ESI-MS of P6-26r (**top trace**) and P7-26r (**bottom trace**) assemblies. (**B**) Thermal unfolding profiles of free P6 (**top trace**) and P6 within P6-26r (**bottom trace**). (**C**) Thermal unfolding profiles of free P7 (**top trace**) and P7 within P7-26r (**bottom trace**). Thermal unfolding of P6 and P7 within the conjugates was generated by subtracting the ellipticity of free 26r at 225 nm from that of the conjugates at all temperatures. Peptide concentration: 100 μM.

The thermal transition profiles of the conjugates became complicated due to the overlap of the CD characteristic peak for 26r at 222 nm and P7/P6 at 225 nm. The molecular structures of P6 and P7 within the conjugates and their temperature-induced unfolding can be extracted by subtracting the CD absorbance of free 26r at 225 nm from that of the conjugate. As shown on the edited melting curve (**Bottom traces** on **Fig. 1B** and **1C** and **Fig. S2**), cooperative thermal transition was still observed for both P6 and P7 with a melting temperature at 46 °C for P6 and 53 °C for P7. Upon conjugation, the melting temperatures of both peptides increased suggesting an enhanced folding of the collagen triple helices. This observation is consistent with a previous report by Woolfson and Brodsky in which the folding of a recombinant bacterial collagen was reinforced upon end to end conjugation with a synthetic coiled coil peptide. [13]

To further examine the solution self-assembly state, we employed small-angle X-ray scattering (SAXS) technique and primarily focused on P7-26r which showed higher thermal stability. The good linear Guinier plot, ln[I(Q)] vs $Q^2$ (**Fig. 2A)**, for SAXS intensities (I(Q)) in the low Q region suggested a good structural homogeneity and one dominating particle size in the solution under study. Using water as the absolute scattering standard, the molecular weight (Mw) was determined to be ~33 kDa based on the forward scattering intensity, I(Q=0), obtained from the Guinier analysis (SI methods).[14] A standard-free and SAXS curve alone method, based on the QI(Q) versus Q plot (**Fig. S3, methods in SI**), was employed to estimate the Mw as ~32 kDa, corresponding to six subunits.[15] The pair-distance distribution function P(r) computed from the SAXS data with the GNOM program[16] showed an asymmetrical Gaussian profile indicating an elongated structure (**Fig. 2B**). To note, the largest dimension of p7-26r assembly is about 13.6 nm as estimated from P(r) function. While SAXS was performed at a relatively high concentration above 500 μM, the self-assembly at lower concentrations was investigated by analytical ultracentrifugation - sedimentation velocity (AUC-SV). **Fig. 2C** showed the raw sedimentation scans taken every ~ 5 mins at 50,000 rpm at a peptide concentration of 100 μM. The distribution of sedimentation coefficients confirmed the predominance of hexamers at 100 μM (**Fig. 2D**), which seem to be in equilibrium with trimers based on the concentration-dependent SV results (**Fig.S4**). We observed prominent trimers as we reduced peptide concentration to 20 μM, as such for cell-based experiments, 50 μM was used to ensure the equilibrium favours the hexamers.

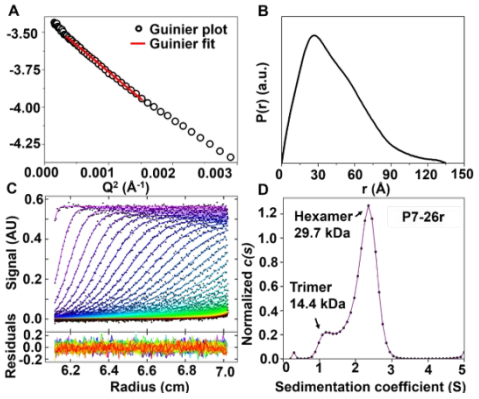


**Figure 2. (A)** Guinier plot of P7-26r assembly in low scattering vector Q region (**B**) The P(r) function computed from the SAXS data with the GNOM program. (**C**) Raw sedimentation profiles of absorbance at 280 nm versus cell radius (**top trace**) and residual plot supplied by SEDFIT software (**bottom trace**). (**D**) Continuous sedimentation coefficient distribution, c(s) curve showing predominance of hexamers mixed with small amounts of trimers. Peptide concentration is 500 μM for SAXS and 100 μM AUC analysis.

To explore the packing and conformation of each domain within the hexamer, we carried out microsecond molecular dynamics (MD) simulations. The initial structure was generated using an in-house Python script with the knowledge of the secondary and tertiary structures reported previously and the CD results presented in this work.[11b] The validity of MD

simulation results was evaluated by comparing the theoretical SAXS profiles of the simulated models with the experimental SAXS data. The goodness-of-fit values ($\chi^2$) were obtained by minimizing the discrepancy between them using FoXS[17] package. During a typical 1-μs MD simulation (**Fig. 3A**), this value was close to 3 in the early stage while fluctuated around 1 with small deviation after 300 ns, suggesting that the simulated structures in the last 700 ns MD trajectories match well with the experimental SAXS result. The comparison between a representative conformation (frame at 988 ns, **Fig. 3C**) adopted by P7-26r in the MD simulation and the experimental SAXS profile is shown in **Fig. 3B**. Using the atomic coordinates, the mean maximum end-to-end distance was found to be 14.1 nm (**Fig. S5**), which matches well with the maximal point-to-point distance at 13.6 nm as estimated from P(r) function (**Fig. 2B**).

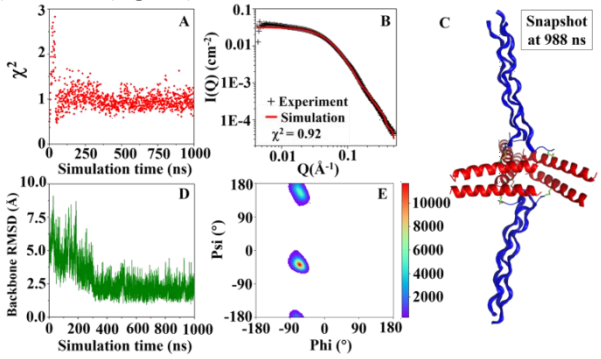


**Figure 3.** Results from a 1-μs molecular dynamics simulation of P7-26r hexamer. (**A**) Plot of goodness-of-fit ($\chi^2$) between FoXS predicted scattering profiles of simulated models and experimental data. (**B**) Comparison of the FoXS predicted scattering of a simulated model (frame at 988 ns) and experimental SAXS profile. (**C**) A representative conformation (frame at 988 ns) adopted by P7-26r. The coiled coils and collagen triple helices domains are shown in red and blue, respectively. (**D**) RMSD of the backbone atoms (C, N, Cα) of the hexamer over the course of simulation. (**E**) Ramachandran plot of the conformational space sampled by P7-26r hexamer during the simulation.

MD simulation provided additional structural features possessed by P7-26r hexamers. The structure averaged from frames in the second 500 ns trajectories was used as the reference conformation to calculate the backbone root mean square deviation (RMSD) that P7-26r hexamer exhibited over the course of the simulation. The backbone RMSD fluctuated vigorously in the first 300 ns (**Fig. 3D**) but stabilized around 2 Å with small deviations from 300 ns to the end of the simulation. Analysis of the backbone RMSD exhibited by different domains showed that the vigorous fluctuation in the early stage was mainly caused by the two collagen triple helices components (**Fig. S6**). Over the course of the entire simulation, the dimeric coiled coils and collagen triple helices were well maintained by P7-26r. Ramachandran plots (**Fig. 3E**) showed that the backbone dihedral angles (φ,ψ) of the coiled coil domains were densely located in the ideal α-helix region and that of the collagen domains were highly populated around the region of an ideal polyproline type II helix secondary structures. Analysis of hydrogen bonds showed that the coiled coil domains exhibited ~88% helicity and the collagen domains retained ~80% of the collagen triple helices adopted by the unconjugated P7 (**Fig. S7**). The overall geometric properties converged after 300 ns (**Fig. S8 and S9**), showing the three coiled coil domains located roughly on the same plane as initially constructed while the collagen triple helices are projected with a ~ 70° angle between the symmetry axis of the collagen domains and the coiled coil plane.

Various peptide-based ligands can be readily incorporated on P7. As a proof-of concept, we used a RGDS ligand which was originally discovered on fibronectin (FN) to interact with the αvβ3 integrin receptor. Notably, the RGDS was found at the N-terminus of FN. To mimic natural FN, we synthesized a new RGDS containing collagen peptides by preferentially having the RGDS at the N-terminus and move the conjugation site of (PCG) to the C-terminus to avoid steric hindrance on RGDS for receptor binding. The new RGDS-containing collagen peptide was conjugated with 26r to form an end-to-side chimeric peptide, termed as (RGDS-P7)-26r (**Scheme-2**).

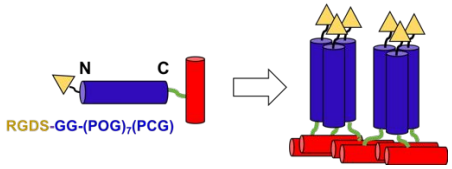


**Scheme 2.** Self-assembly of RGDS containing chimeric peptides into hexamers with control over local (trimer) and global (hexamer) multivalent ligand presentation.

The formation of hexamer was confirmed by AUC (**Fig. S10**) and further supported by the MD simulation study (**Fig. S11**). Cytotoxicity of (RGDS-P7)-26r was evaluated using human glioblastoma U87MG cells which are known to express high levels of the integrin receptor, αvβ3.[19] As shown in **Fig. S12**, the cell viability maintained at ~85% at peptide concentrations up to 100 μM. To demonstrate tumor targeted efficacy, we synthesized several variants of chimeric peptides which can adopt different oligomerization states. By disrupting the (POG) repeating pattern, we synthesized a constitutional isomer of P7, termed as P7sr which did not fold into a collagen triple helix given the absence of the corporative thermal transition profile (**Fig. S13**). The chimeric peptide, (RGDS-P7sr)-26r is expected to only form a dimer. Similarly, a trimeric assembly can be generated by (RGDS-P7)-26r(P) in which 26r(P) was synthesized by replacing the hydrophobic residues on 26r with proline to form a monomeric random coil. The absence of a tertiary structure was confirmed by the thermal transition study (**Fig.S14**). A control hexamer was prepared by using P7-26r without RGDS ligand or with DGSR. All chimeric peptides were labelled with FITC at the N-terminus of either 26r or 26r(P). We compared the cell uptake by monitoring the intracellular fluorescence after 24 hrs of incubation of peptides with U87MG cells. As shown in **Fig.4**, (RGDS-P7)-26r showed much higher fluorescence intensity than assemblies with bivalent and trivalent RGDS ligand presentation. Without RGDS, P7-26r showed some cell uptake, however much lower than (RGDS-P7)-26r. Ligand targeting was further supported by the low cell uptake of (RGDS-P7)-26r when incubated with NIH/3T3 mouse fibroblasts which do not have the integrin receptor as well as (DGSR-P7)-26r with a scrambled targeting sequence (**Fig. S15 and S16**). While we are performing a more systematic cell targeting study using a panel of different targeting ligands, current results suggest that by controlling

both local and global ligand presentation, tumor targeting efficacy can be enhanced.

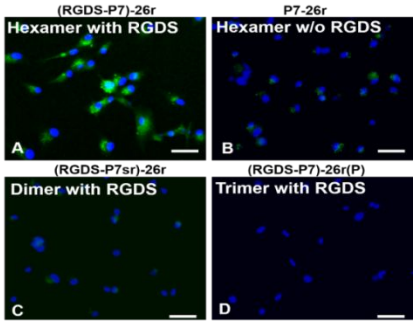


**Figure 4.** Fluorescence images of U87MG cells treated with FITC labeled peptides. (**A**) (RGDS-P7)-26r (**hexamer**), (**B**) P7-26r (**hexamer w/o RGDS**), (**C**) (RGDS-P7sr)-26r (**dimer**) and (**D**) (RGDS-P7)-26r(P) (**trimer**). Incubation time: 24 hrs. Peptide concentration: 50 μM. Scale bar: 100 μm. Green: FITC labeled peptides. Blue: Hoechst 33342 staining.

In summary, we have demonstrated a hexameric peptide nanostructure based on the self-assembly of a chimeric peptide consisting of two distinctly folded domains. Tumor targeted hexamers were fabricated with precise control over both the local and global ligand presentation. *In vitro* tumor targeting efficacy was much higher for ligand functionalized hexamers than dimers or trimers, as well as hexamers without targeting ligands. These molecularly defined hexamers are promising candidates for the generation of artificial antibodies which can combine various imaging modalities and chemo- and photothermal- therapeutics for a range of disease diagnosis and treatment.

The work was supported by the University of Texas at Arlington. We would like to thank Chad Brautigam and Shih-Chia Tso at the Biophysical core facilities of UT Southwestern Medical School for the excellent technical support and kind discussions on the AUC experiment and data analysis. This work was supported in part through the NYU IT High Performance Computing resources, services and staff expertise. The SAXS measurements were performed at Beamline 12-ID-B of the Advanced Photon Source, a U.S. Department of Energy (DOE) Office of Science User Facility operated for the DOE Office of Science by Argonne National Laboratory under Contract No. DE-AC02-06CH11357. This work was supported by the National Science Foundation (Award CHE-1507946 to K.K.).

## Conflict of interest

There are no conflicts to declare.

## Notes and references

1. a) L. K. Bogart, G. Pourroy, C. J. Murphy, V. Puntes, T. Pellegrino, D. Rosenblum, D. Peer and R. Lévy, *ACS Nano*, 2014, **8**, 3107-3122; b) M. Ferrari, *Nat. Rev. Cancer*, 2005, **5**, 161-171.
2. a) R. Chakrabarty, P. S. Mukherjee and P. J. Stang, *Chem. Rev.*, 2011, **111**, 6810-6918; b) Y.-b. Lim, K.-S. Moon and M. Lee, *Chem. Soc. Rev.*, 2009, **38**, 925-934.
3. a) N. P. King, J. B. Bale, W. Sheffler, D. E. McNamara, S. Gonen, T. Gonen, T. O. Yeates and D. Baker, *Nature*, 2014, **510**, 103-108; b) Y.-T. Lai, D. Cascio and T. O. Yeates, *Science*, 2012, **336**, 1129; c) N. C. Seeman and H. F. Sleiman, *Nat. Rev. Mater.*, 2017, **3**, 17068.
4. a) H. Acar, S. Srivastava, E. J. Chung, M. R. Schnorenberg, J. C. Barrett, J. L. LaBelle and M. Tirrell, *Adv. Drug Deliv. Rev.*, 2017, **110-111**, 65-79; b) L. Adler-Abramovich and E. Gazit, *Chem. Soc. Rev.*, 2014, **43**, 6881-6893; c) A. L. Boyle, E. H. Bromley, G. J. Bartlett, R. B. Sessions, T. H. Sharp, C. L. Williams, P. M. Curmi, N. R. Forde, H. Linke and D. N. Woolfson, *J. Am. Chem. Soc.*, 2012, **134**, 15457-15467; d) H. Cui, M. J. Webber and S. I. Stupp, *J. Pept. Sci.*, 2010, **94**, 1-18; e) G. A. Hudalla, T. Sun, J. Z. Gasiorowski, H. Han, Y. F. Tian, A. S. Chong and J. H. Collier, *Nat. Mater.*, 2014, **13**, 829-836; f) K. Nagy-Smith, E. Moore, J. Schneider and R. Tycko, *Proc. Natl. Acad. Sci. U.S.A.*, 2015, **112**, 9816-9821; g) S. Sathaye, H. Zhang, C. Sonmez, J. P. Schneider, C. M. MacDermaid, C. D. Von Bargen, J. G. Saven and D. J. Pochan, *Biomacromolecules*, 2014, **15**, 3891-3900.
5. a) J. M. Fletcher, R. L. Harniman, F. R. H. Barnes, A. L. Boyle, A. Collins, J. Mantell, T. H. Sharp, M. Antognozzi, P. J. Booth, N. Linden, M. J. Miles, R. B. Sessions, P. Verkade and D. N. Woolfson, *Science*, 2013, **340**, 595-599; b) J. F. Ross, A. Bridges, J. M. Fletcher, D. Shoemark, D. Alibhai, H. E. V. Bray, J. L. Beesley, W. M. Dawson, L. R. Hodgson, J. Mantell, P. Verkade, C. M. Edge, R. B. Sessions, D. Tew and D. N. Woolfson, *ACS Nano*, 2017, **11**, 7901-7914.
6. a) H. Gradišar, S. Božič, T. Doles, D. Vengust, I. Hafner-Bratkovič, A. Mertelj, B. Webb, A. Šali, S. Klavžar and R. Jerala, *Nat. Chem. Biol.*, 2013, **9**, 362-366; b) F. Lapenta, J. Aupič, Ž. Strmšek and R. Jerala, *Chem. Soc. Rev.*, 2018, **47**, 3530-3542; c) A. Ljubetič, F. Lapenta, H. Gradišar, I. Drobnak, J. Aupič, Ž. Strmšek, D. Lainšček, I. Hafner-Bratkovič, A. Majerle, N. Krivec, M. Benčina, T. Pisanski, T. Ć. Veličković, A. Round, J. M. Carazo, R. Melero and R. Jerala, *Nat. Biotechnol.*, 2017, **35**, 1094-1101.
7. E. De Santis, H. Alkassem, B. Lamarre, N. Faruqui, A. Bella, J. E. Noble, N. Micale, S. Ray, J. R. Burns, A. R. Yon, B. W. Hoogenboom and M. G. Ryadnov, *Nat. Commun.*, 2017, **8**, 2263.
8. a) A. G. Kreutzer and J. S. Nowick, *Acc. Chem. Res.*, 2018, **51**, 706-718; b) P. J. Salveson, S. Haerianardakani, A. Thuy-Boun, A. G. Kreutzer and J. S. Nowick, *J. Am. Chem. Soc.*, 2018, **140**, 5842-5852; c) R. K. Spencer, H. Li and J. S. Nowick, *J. Am. Chem. Soc.*, 2014, **136**, 5595-5598.
9. a) T. Jiang, C. Xu, X. Zuo and V. P. Conticello, *Angew. Chem. Int. Ed.*, 2014, **53**, 8367-8371; b) T. Jiang, C. Xu, Y. Liu, Z. Liu, J. S. Wall, X. Zuo, T. Lian, K. Salaita, C. Ni, D. Pochan and V. P. Conticello, *J. Am. Chem. Soc.*, 2014, **136**, 4300-4308.
10. a) B. H. San, J. Hwang, S. Sampath, Y. Li, L. L. Bennink and S. M. Yu, *J. Am. Chem. Soc.*, 2017, **139**, 16640-16649; b) F. W. Kotch and R. T. Raines, *Proc. Natl. Acad. Sci. U.S.A.*, 2006, **103**, 3028-3033; c) J. A. Fallas and J. D. Hartgerink, *Nat. Commun.*, 2012, **3**, 1087.
11. a) L. Jiang, D. Xu, K. E. Namitz, M. S. Cosgrove, R. Lund and H. Dong, *Small*, 2016, **12**, 5126-5131; b) L. Jiang, S. Yang, R. Lund and H. Dong, *Biomater. Sci.*, 2018, **6**, 272-279.
12. T. Yokota, D. E. Milenic, M. Whitlow and J. Schlom, *Cancer Res.*, 1992, **52**, 3402-3408.
13. A. Yoshizumi, J. M. Fletcher, Z. Yu, A. V. Persikov, G. J. Bartlett, A. L. Boyle, T. L. Vincent, D. N. Woolfson and B. Brodsky, *J. Biol. Chem.*, 2011, **286**, 17512-17520.
14. C. D. Putnam, M. Hammel, G. L. Hura and J. A. Tainer, *Q. Rev. Biophys.*, 2007, **40**, 191-285.
15. R. P. Rambo and J. A. Tainer, *Nature*, 2013, **496**, 477-481.
16. A. V. Semenyuk and D. I. Svergun, *J. Appl. Crystallogr.*, 1991, **24**, 537-540.
17. a) D. Schneidman-Duhovny, M. Hammel, John A. Tainer and A. Sali, *Biophys. J.*, 2013, **105**, 962-974; b) D. Schneidman-Duhovny, M. Hammel, J. A. Tainer and A. Sali, *Nucleic Acids Res.*, 2016, **44**, W424-W429.
18. a) W. Liu, G. Hao, M. A. Long, T. Anthony, J.-T. Hsieh and X. Sun, *Angew. Chem. Int. Ed.*, 2009, **48**, 7346-7349; b) E. Ruoslahti, *Annu. Rev. Cell Dev. Biol.*, 1996, **12**, 697-715.
19. Z. Liu, F. Wang and X. Chen, *Drug Dev. Res.*, 2008, **69**, 329-339.

# Graphical Abstract

## Self-assembly of Chimeric Peptides Toward Molecularly Defined Hexamers with Controlled Multivalent Ligand Presentation

Xiushuang Yuan[‖], Linhai Jiang[‖], Weike Chen, Bo Song, Wei Chen, Xiaobing Zuo, Xiankai Sun, Xiaopeng Li, Kent Kirshenbaum, Shizhong Luo, He Dong*

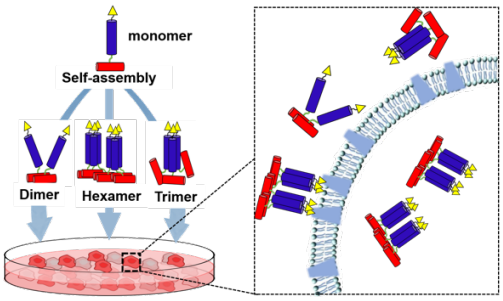


In this work, we report the self-assembly of chimeric peptides in which two distinctly folded domains can be organized into a finite peptide hexamer for precise control over multivalent ligand presentation and enhanced tumor cell targeting.